HRVAS: Heart Rate Variability Analysis Software

This document is in "beta" mode. Thus it is a work in progress. If the information that you need isn't listed or isn't clearly stated, please contact the author.

Updated – 12/2/2014

Please reference the following thesis if citing any of this work:

Contact Information:

John T. Ramshur
University of Memphis
Department of Biomedical Engineering
Memphis, TN
jramshur@gmail.com
jramshur@memphis.edu

Contents

1 Description

HRVAS is a MATLAB application for performing HRV analysis. A single GUI is used to choose analysis options and to display results. HRVAS includes time-domain, frequency-domain, Poincare', non-linear, and time-frequency HRV analysis. HRVAS also features IBI preprocessing, batch processing and export tools.

2 Installation

Below are instructions for the two installation types available for HRVAS. Type 1 describes how to install HRVAS for use without MATLAB. Type 2 describes how to install/setup HRVAS if you have already have MATLAB. If you don't know what MATLAB is…then Type 1 is for you.

2.1 Type 1: Standalone Application

Software Dependencies: Software needed to run HRVAS

MATLAB v2008 or higher - Older versions probably work as long as it's not too old. If you don't have MATLAB, please contact the author about a stand-alone version.

2.1.1 How to Install

1. Install the MATLAB Compiler Runtime (MCR). Download and run MCRInstaller.exe. MCR is needed to allow HRVAS to run outside of the MATLAB environment.

2. Unzip the HRVAS_v1.0.1.zip package. Run HRVAS.exe to open the user interface.

2.2 Type 2: MATLAB Source Code

These dependencies must be present and/or installed before using ECG Viewer.

Software Dependencies: Software needed to run HRVAS

1. MATLAB v2008 or higher - Older versions probably work as long as it's not too old. If you don't have MATLAB, please use the stand-alone version.

MATLAB Toolbox Dependencies: Toolboxes needed to run *certain aspects* of HRVAS

1. MATLAB Signal Processing Toolbox (needed for frequency analysis)
2. MATLAB Wavelet Toolbox (*OPTIONAL*, needed IF using wavelet filtering)

File Dependencies: other files needed to run ECG Viewer

1. HRVAS.m - primary GUI for HRVAS

2. timeFreqHRV.m – time-frequency HRV function
3. poincareHRV.m – Poincare HRV function
4. timeDomainHRV.m – time-domain HRV function
5. freqDomainHRV.m – freq-domain HRV function
6. nonlinearHRV.m – nonlinear HRV function
7. locateOutliers.m - locates IBI outliers or ectopic beats
8. batchHRV.m – batch processing function
9. exportHRV.m – function to export HRV
10. ellipsedraw.m – draws ellipse for Poincare plots (by another author)
11. lomb2.m – computes Lomb-Scargle PSD
12. preProcessIBI.m – function to preprocess IBI
13. replaceOutliers.m – function that replaces IBI outliers
14. slidingWindow.m – function to get increments for sliding window
15. wavelet.m – wavelet functions (by another author)

2.2.1 How to Install

1. Unzip the HRVAS_v1.0.0.zip package. Run the main.m file within MATLAB to open the user interface.

3 Quick Start Guide

1. Select an IBI data file.
2. Adjust analysis options
3. Preview IBI or Run Analysis
    1. Click “Preview” to see a preview of the preprocessed IBI signal.
    2. Click “Run” to generate HRV results.
4. Select a tab to see results for that analysis method.
5. Export HRV results … if needed.

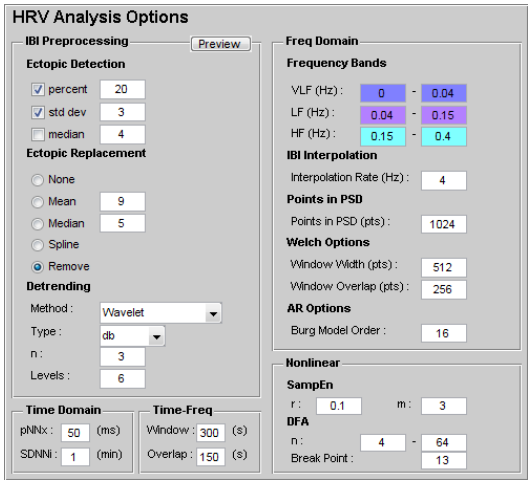
HRV Analysis Options
IBI Preprocessing
Preview
Ectopic Detection
percent 20
std dev 3
median 4
Ectopic Replacement
None
Mean 9
Median 5
Spline
Remove
Detrending
Method : Wavelet
Type : db
n : 3
Levels : 6
Time Domain
pNNx : 50 (ms)
SDNNi : 1 (min)
Time-Freq
Window : 300 (s)
Overlap : 150 (s)
Freq Domain
Frequency Bands
VLF (Hz) : 0 - 0.04
LF (Hz) : 0.04 - 0.15
HF (Hz) : 0.15 - 0.4
IBI Interpolation
Interpolation Rate (Hz) : 4
Points in PSD
Points in PSD (pts) : 1024
Welch Options
Window Width (pts) : 512
Window Overlap (pts) : 256
AR Options
Burg Model Order : 16
Nonlinear
SampEn
r : 0.1
m : 3
DFA
n : 4 - 64
Break Point : 13

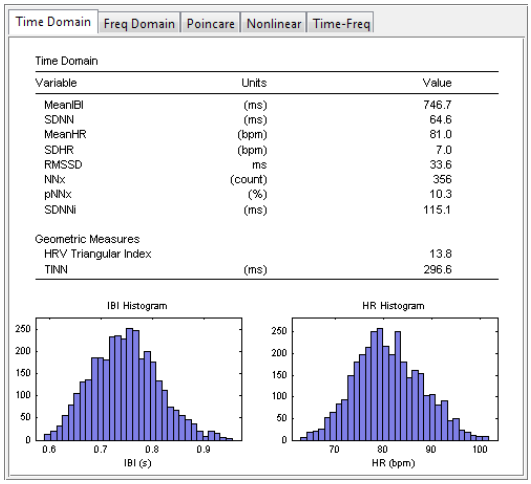
Time Domain
Freq Domain
Poincare
Nonlinear
Time-Freq
Time Domain
Variable Units Value
MeanIBI (ms) 746.7
SDNN (ms) 64.6
MeanHR (bpm) 81.0
SDHR (bpm) 7.0
RMSSD ms 33.6
NNx (count) 356
pNNx (%) 10.3
SDNNi (ms) 115.1
Geometric Measures
HRV Triangular Index 13.8
TINN (ms) 296.6
IBI Histogram
IBI (s)
HR Histogram
HR (bpm)

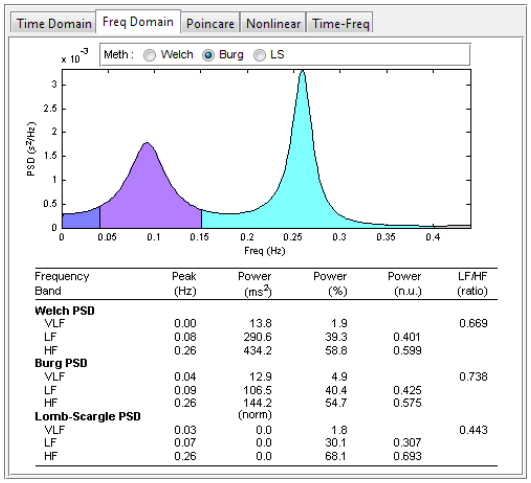

Frequency Band	Peak (Hz)	Power (ms^2)	Power (%)	Power (n.u.)	LF/HF (ratio)
Welch PSD					
VLF	0.00	13.8	1.9		0.669
LF	0.08	290.6	39.3	0.401	
HF	0.26	434.2	58.8	0.599	
Burg PSD					
VLF	0.04	12.9	4.9		0.738
LF	0.09	106.5	40.4	0.425	
HF	0.26	144.2	54.7	0.575	
Lomb-Scargle PSD		(norm)			
VLF	0.03	0.0	1.8		0.443
LF	0.07	0.0	30.1	0.307	
HF	0.26	0.0	68.1	0.693	

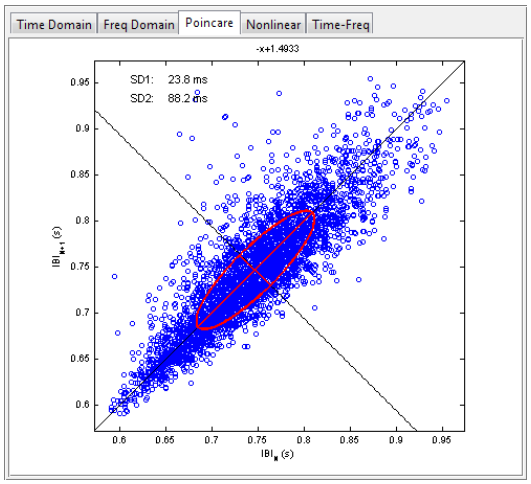

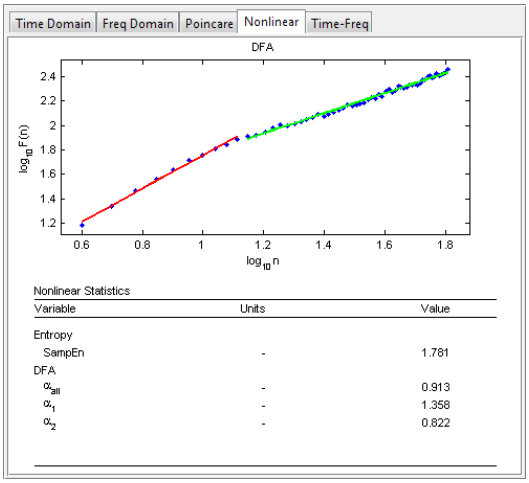

Nonlinear Statistics

Variable	Units	Value
Entropy		
SampEn	-	1.781
DFA		
α_{all}	-	0.913
α_1	-	1.358
α_2	-	0.822

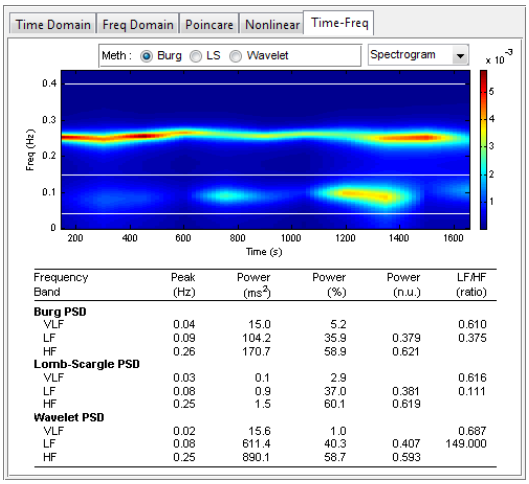

Frequency Band	Peak (Hz)	Power (ms^2)	Power (%)	Power (n.u.)	LF/HF (ratio)
Burg PSD					
VLF	0.04	15.0	5.2		0.610
LF	0.09	104.2	35.9	0.379	0.375
HF	0.26	170.7	58.9	0.621	
Lomb-Scargle PSD					
VLF	0.03	0.1	2.9		0.616
LF	0.08	0.9	37.0	0.381	0.111
HF	0.25	1.5	60.1	0.619	
Wavelet PSD					
VLF	0.02	15.6	1.0		0.687
LF	0.08	611.4	40.3	0.407	149.000
HF	0.25	890.1	58.7	0.593	

4 Misc. Information

4.1 Input Data

HRVAS can read inter-beat interval files (.ibi) and text files (.txt), both of which are ASCII files. The expected data format must have one or two columns. If one column is used, this column must represent IBI/RR values in units of seconds. If two columns are used, the first column represents time in units of seconds. The second column represents IBI/RR values in units of seconds

4.2 Exporting Results

1. Export HRV Results – exports HRV results to a MS Excel file.
2. Exporting IBI
    a. Export IBI – exports currently loaded IBI
    b. Export IBI (ibi only) – exports IBI values only. Time values are not exported.
    c. Export IBI (processed) – exports preprocessed IBI.

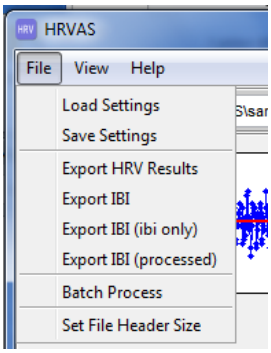

4.3 Batch Processing

File>Batch Processing

1. Choose directory.
2. Select files. Uncheck the checkbox labeled “Include all files” to select individual files for batch processing.
3. Run Batch.

5 HRV Analysis & Preprocessing

This chapter describes several analysis methods used by HRVAS. The first section describes techniques used to process IBI time series prior to HRV analysis. The remaining four sections describe four major categories of HRV analysis and include: time based metrics (e.g., variance); frequency based metrics that

evaluate powers or ratios of powers within certain frequency bands; nonlinear based metrics that evaluate complexity and self-similarity; and time-frequency metrics that expand on frequency based metrics by monitoring them through time. For alternative overviews of HRV analysis see articles by Seely, et al. [1], Acharya, et al. [2], Berntson, et al. [3], and Malik, et al. [4].

5.1 Analysis Quick Start Guide

This section will give a table layout of all the analyses used by HRVAS and their references.

			Description	Reference
Preprocessing	Ectopic Detection	Percent		
		Standard Dev.		
		Mean		
	Ectopic Replacement	Mean		
		Median		
		Spline		
		None		
	Detrending	Wavelet		
		Matlab Smooth		
		Polynomial		
		Wavelet Packet		
		Smoothness Priors		
HRV Analysis	Time Domain	Mean		
		SDNN		
		SDNNi		
		NNx, pNNx		
		HRVti		
		TINN		
	Freq. Domain	NOTES:	Talk about burg, welch, and LS	
		Peak VLF, LF, HF		
		VLF, LF, HF		
		pVLF, pLF, pHF		
		nLF, nHF		
		LF/HF Ratio		
	Time Freq	NOTES:		
		rLFHF		
	Nonlinear			

	Pointcare			

5.2 Analysis Options Guide

Talk about the options included in the GUI.

5.3 IBI Extraction

Data series used in HRV analysis are time series containing beat-to-beat intervals extracted from ECG signals. Temporal locations of beats are frequently based on the R-wave because it is often the easiest wave to distinguish. R waves typically have the largest amplitudes compared to surrounding P, Q, S, and T waveforms. Thus a beat-to-beat interval can be defined as the time difference between consecutive R peaks (RR interval). Because the R wave is not the only temporal marker for beat locations, e.g. QRS complex, some use the term IBI as a generalization to represent any beat-to-beat intervals. Additionally, RR intervals originating from normal sinus rhythms are sometimes referred to as NN (normal-to-normal) intervals. Thus, standard nomenclature of "NN" is used in place of IBI or RR to indicate IBI's containing no ectopic intervals. Many authors, including this research, interchangeably use IBI, RR, or NN (normal-to-normal) to represent IBI series assuming ectopic beats have been corrected.

Figure 5.1 shows a hypothetical ECG and how IBI's are determined based on R waves. IBI(1) and IBI (2) represent the first and second data point of the IBI time series signal. The IBI time series of an ECG segment containing N beats is given by

$$IBI(n) = beat(n+1) - beat(n) : 1 \le n \le N-1 \qquad (2.1)$$

where beat(n) is the time location of the nth beat.

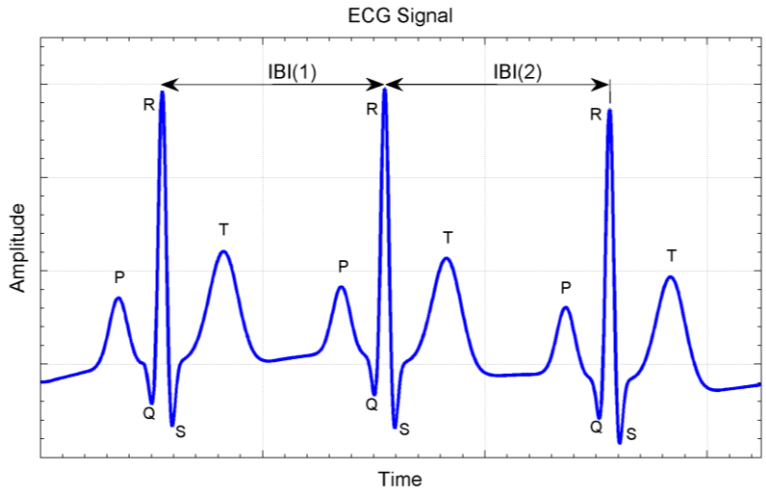

Figure 5.1 – Determination of IBI. Simulated ECG containing three beats with arbitrary units of time and amplitude. Time intervals corresponding to the IBI are indicated by IBI(1) and IBI(2). ECG morphology is shown by five characteristic waves P, Q, R, S, and T.

5.4 Preprocessing

Preprocessing of IBI time series data is frequently required before HRV analysis to reduce analysis errors. The three primary types of IBI preprocessing are ectopic beat/interval correction, detrending, and IBI resampling. HRV analysis errors due to ectopic beats and IBI trends have been reported by Thuraisingham [5] and Colak [6]. In the context of IBI, ectopic beats refer to any IBI based on one or more abnormal beats. Any abnormal IBI that is due to either a false/missed beat, fiducial point misalignment, or cardiac ectopy may be considered ectopic.

IBI time series also contain slowly varying trends that are generally assumed to be inherent to most biological signals including IBI. Some HRV analysis methods assume that IBI signals are stationary or absent of low frequency trends. Specifically, power spectrum estimations based on Fourier transform require that the random variable of interest be wide sense stationary (the mean does not change with time) [7]. To alleviate any non-stationarities within IBI time series, detrending is often used before HRV analysis [6, 8, 9]. In addition to stationarity, these methods require evenly sampled IBI, which is inherently not the case for IBI signals. Figure 5.2 illustrates an IBI time series before and after removing both ectopic intervals and low frequency

trend.

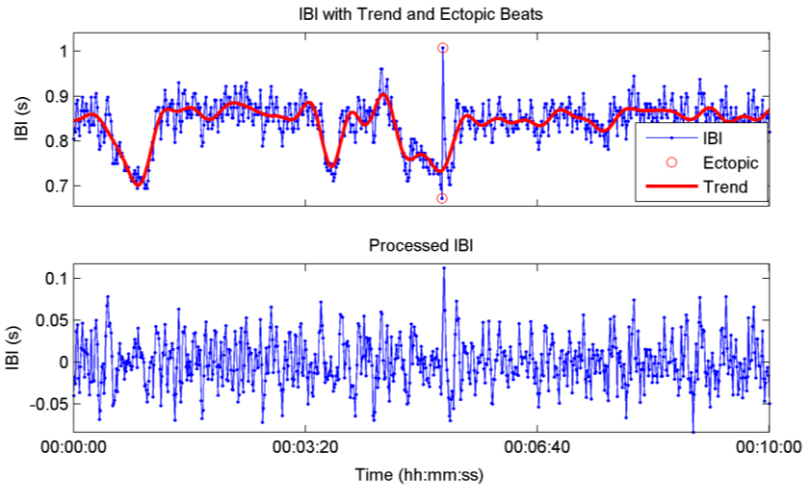

Figure 5.2 – IBI signal before and after detrending and ectopic interval removal.

IBI time series from healthy human.

5.4.1 Ectopic Interval Detection

Before ectopic intervals can be corrected they must first be detected or marked. Here three detection techniques are discussed. Although the term filter is used in this section, no change to the original IBI occurs during ectopic interval detection. The percentage filter locates intervals that change by more than a user defined percentage (often 20%) from the previous interval [10]. This method locates any sudden or abrupt IBI changes. Another method used to detect ectopic intervals is the standard deviation filter which marks outliers as being intervals that lie beyond the overall mean IBI by a user defined value of standard deviations (often 3 SD) [10]. Lastly, the median filter acts as an impulse rejection filter with threshold to delineate ectopic intervals [5]. The median filter of a random variable *x* of length *N* using a threshold of τ is given by

$$D(n) = \frac{\left|x(n) - med(x)\right|}{1.483 \cdot med\left\{\left|x(n) - med(x)\right|\right\}} \qquad (2.2)$$

if $D(n) \geq \tau$, then not ectopic; else ectopic

5.4.2 Ectopic Interval Correction

Four correction techniques are described to replace ectopic intervals found during the detection process. The first technique is to simply remove any ectopic intervals found. Simple ectopic interval removal has been shown to be as effective as other replacement methods [11]. Another method replaces any ectopic interval with the mean value of *w* neighboring IBI intervals centered on the ectopic interval using Equation(2.3) . Similarly, the median method replaces ectopic intervals with the median value of *w* neighboring IBI intervals centered on the ectopic interval using Equation (2.4) [5]. Lastly, cubic spline replacement replaces ectopic intervals using cubic spline interpolation.

$$ibi'(n) = mean\left\{ibi(n+m) : |m| \le \frac{w-1}{2}\right\} \quad (2.3)$$

$$ibi'(n) = med\left\{ibi(n+m) : |m| \le \frac{w-1}{2}\right\} \quad (2.4)$$

5.4.3 IBI Detrending

Several methods of detrending exist in the literature to remove low frequency trends including: linear detrending, polynomial detrending, wavelet detrending, wavelet packet detrending, and smoothing priors detrending.

5.4.4 Linear and Polynomial Detrending

Two of the simplest methods used for detrending IBI series are linear and polynomial detrending [12-14]. Linear detrending is accomplished by removing a linear least-squares-fit from the IBI series. Similarly, polynomial detrending removes a second or third order polynomial fit (in a least squares sense) from the IBI series.

5.4.4.1 Wavelet Detrending

Wavelet detrending is accomplished by decomposing the original IBI time series into a tree of approximation and detail coefficients using discrete wavelet transform (DWT) (see Section 5.7.2.2). Each decomposed sub-band is associated with a range of frequencies with the highest level of approximation containing the lowest frequencies. Removing the low frequency trend can be accomplished by two methods. The first method sets all the wavelet coefficients of the highest level approximation (lowest frequency) to zero, and then performs an inverse DWT. The alternative method reconstructs only the highest approximation

sub-band which is then subtracted from the original IBI series [5]. Either method effectively applies signal detrending.

5.4.4.2 Wavelet Packet Detrending

Detrending using wavelet packets works similar to the detrending method based on DWT mentioned in the previous section. Instead of decomposing the signal using DWT the discrete wavelet packet transform (DWPT) is used (see Section 5.7.2.2). Wavelet coefficients of sub-bands that contain frequency components of any unwanted trend are set to zero. Reconstruction of the IBI series using inverse DWPT produces a detrended IBI series [15].

Commented [J1]: Only mentioned one method to detrend with dwpt

5.4.4.3 Smoothing Priors

The final detrending method to be discussed is the smoothing priors approach [15, 16]. In the smoothing priors approach a N-1 long, an equally sampled IBI time series is represented as the combination of stationary and trend components, $z = z_{stationary} + z_{trend}$. This method computes a stationary signal from the original. The estimated stationary component is written as

$$\hat{z}_{stationary} = z - \mathbf{H}\hat{\boldsymbol{\theta}}_{\lambda} = \left(\mathbf{I} - \left(\mathbf{I} + \lambda^2 \mathbf{D}_2^T \mathbf{D}_2\right)^{-1}\right) z \qquad (2.5)$$

where $\mathbf{H} \in \mathbf{R}^{(N-1)\text{x}M}$ is the observation matrix. For simplification, an identity matrix is used in place of the observation matrix $\mathbf{H}$. $\hat{\boldsymbol{\theta}}_{\lambda}$ represents the estimate of the regression parameters with λ as the regularization parameter and $\mathbf{D}_2 \in \mathbf{R}^{(N-3)\text{x}(N-1)}$ is the second order difference matrix.

5.4.5 IBI Resampling

In addition to most Fourier based power spectrum estimates (see Chapter 5.6) requiring signal stationarity; they also require time series that are regularly sampled in time. Spectrum estimates taken from irregularly time sampled signals can introduce additional harmonics into the power spectrum [17]. For this reason, IBI time series must be resampled prior to some power spectrum estimates. Commonly used resampling schemes are cubic spline and linear interpolation [18].

5.5 Time-Domain Analysis

5.5.1 Statistical Measures

Time domain HRV analyses are often classified as statistical or geometric methods. Statistical time-domain measures are statistical based measures calculated directly from the IBI series. Time domain measures include: mean IBI, the standard deviation of the NN interval series (SDNN), the root mean square of successive differences of the IBI series (RMSSD), the number of successive differences that are greater than *x* milliseconds (NNx), and the percentage of total intervals that successively differ by more than *x* milliseconds (pNNx) [19].

Two variants of the SDNN are used with longer datasets. The first step in both of these variations involves separating the IBI series into non-overlapping segments. For human IBI's the segment lengths are often five minutes [4]. The first variant is the SDNN index or SDNNi, Equation (2.6) , and is computed by finding the standard deviation of each IBI segment and then returning the mean value of standard deviations. The SDANN measure is computed in the opposite manner, Equation (2.7). SDANN computes the mean IBI of each segment and then returns the standard deviation of all means. SDNNi and SDANN are represented mathematically using the following equations:

$$SDNNi = \frac{1}{M}\sum_{i=1}^{M} SDNN\left(i\right) \tag{2.6}$$

$$SDANN = \sqrt{\frac{1}{M-1}\sum_{i=1}^{M}\left[meanIBI\left(i\right) - \overline{meanIBI}\right]^2} \tag{2.7}$$

where SDNN(i) represents the SDNN value of the i^{th} IBI segment, meanIBI(i) represent the mean IBI value of the i^{th} IBI segment, and *M* is the total number of segments.

5.5.2 Geometric Measures

Geometric HRV measures are based on calculations taken from a geometric pattern who's basis lies with the IBI series [4]. The most common geometric pattern used is the histogram of IBI. Two measures based on the IBI histogram are the HRV triangular index (HRVti) and the triangular interpolation of the NN interval histogram (TINN). Figure 5.3 represents the histogram of a hypothetical IBI series where *D(t)* is the density distribution of IBI. The maximum value of *D(t)* is represented by *Y* and is located at *t=X.* HRVti is the value obtained by dividing the area integral of *D(t)* by the maximum value *Y*. If the distribution *D(t)* is on a discrete

horizontal scale then the area integral is just the total number of IBI intervals N_{IBI}. Therefore HRVti is obtained by

$$HRVti = \frac{N_{IBI}}{Y}. \qquad (2.8)$$

For the computation of TINN the values *N* and *M* are established on the time axis and a triangular function *q(t)* constructed such that *q(t)=0* for $M \leq t \leq N$. The peak of the triangle occurs at q(*X*)=*Y*. The triangle base defined by M and N are determined by minimizing the integral $\int_0^{+\infty} (D(t) - q(t))^2 dt$. Finally, TINN is expressed in milliseconds and computed using [4]

$$TINN = M - N. \qquad (2.9)$$

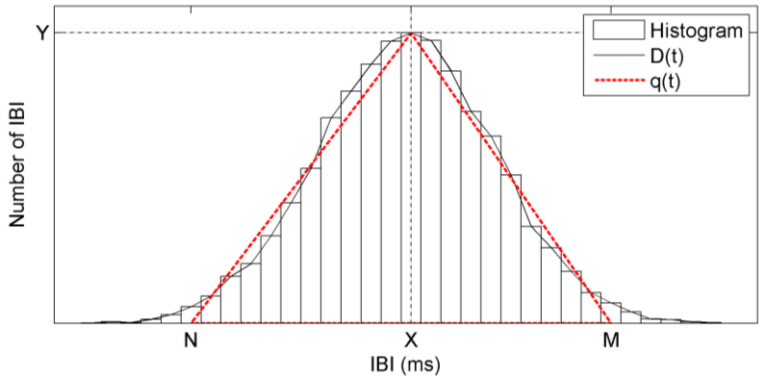

Figure 5.3 – Histogram of hypothetical IBI time series. D(t) represents the sample distribution. q(t) represents a triangular function fitted to D(t) by minimizing the integral of the squared difference between D(t) and q(t). Y = D(X) = max(D).

5.6 Frequency-Domain Analysis

Fluctuations in HR are often thought to be periodic and occurring on many time scales [20]. Quantifying these fluctuations within the IBI time series can be done by calculating the power spectrum density (PSD). The

PSD presents spectral power density of a time series as a function of frequency. Therefore, PSD estimates can give information about the amount of power in which certain frequencies contribute to a time series.

In general, frequency-domain HRV analysis is concerned with four previously mentioned frequency oscillations or bands [4]: ULF, VLF, LF, and HF. For humans ULF, VLF, LF, and HF frequency bands are defined to be 0-0.0033 Hz, 0.003-0.04 Hz, 0.04-0.15 Hz, and 0.15-0.4 Hz respectively. The ULF and VLF are often ignored due to the lack of long data recordings needed to accurately resolve these frequencies or due to the use of IBI detrending techniques that may destroy information within those bands.

Typical HRV measures taken from frequency-domain analysis are powers within frequency bands and ratios of powers. The amount of power contained within a frequency band is obtained by integrating the PSD between the band frequency limits. Measures of spectral power are reported as absolute (aVLF, aLF, aHF), percentage of the sum of aLF and aHF (pLF, pHF), or normalized to total power (nLF, nHF). In addition to the power measures, the ratio of LF to HF (LFHF) provides a so called sympatho-vagal balance. Finally, less commonly mentioned measures are the peak frequencies within the VLF, LF, and HF bands.

Estimating the PSD can be performed using many methods, but methods based on Fast-Fourier Transform (FFT) and autoregressive (AR) modeling are perhaps the most popular in spectral analysis of HRV [20]. Classical power spectrum estimates developed by Bartlett (1948), Blackman and Tukey (1958), and Welch (1967) are examples of methods based on FFT [21]. Because the FFT makes no assumptions on how the data are generated the classical methods are often referred to as non-parametric. The AR power spectrum methods do make assumptions and are therefore called parametric. Contributing to the popularity of the FFT based estimates are their simplicity, broad understanding, and ease of computation using modern computers and software.

However, both FFT and AR based PSD estimates have prerequisites that are seldom if ever met by biological signals such as cardiac IBI series [22]. Both methods require the analyzed time signal to be stationary and evenly sampled, which is inherently not the case with IBI signals [7, 21]. The commonly used linear and cubic spline resampling were shown to overestimate the LFHF ratio with an error that is greater than the error between population differences [23]. Consequently, other methods such as the Lomb-Scargle periodogram and methods based on wavelet transforms are becoming popular [24-29]. Lomb-Scargle does not require resampling and wavelet transform based estimates do not require stationarity [30]. Despite the aforementioned limitations of FFT and AR based PSD estimates, they are widely used in HRV.

5.6.1 Welch Periodogram

To understand Welch's periodogram one must first understand the discrete Fourier transform (DFT), the basic periodogram, and the modified periodogram. The N-point DFT of a random variable *X(n)* is given by

$$DFT_x(f) = \sum_{n=0}^{N-1} X(n) e^{-i2\pi fn} \qquad (2.10)$$

Practical computations of the DFT use the FFT for speed advantages. The periodogram, extension of the DFT, is a basic method of estimating power spectral density of a time series and is given by

$$P(f) = \frac{1}{N}\left|\sum_{n=0}^{N-1} X(n) e^{-i2\pi fk/L}\right|^2 \quad \text{k=0,1,...,L-1.} \qquad (2.11)$$

Reducing spectral leakage of the periodogram can be accomplished by incorporating a weighted windowing function *w(n)*, e.g. Hamming and Hanning, to the input series. Data near the edges of the time series are given less weight compared to data nearer the center. Thus, the modified periodogram is given by

$$P_M(f) = \frac{1}{MU}\left|\sum_{n=0}^{M-1} X(n) w(n) e^{-i2\pi fn}\right|^2 \quad \text{i=0,1,...,L-1} \qquad (2.12)$$

where $U = 1/M \sum_{n=0}^{M-1} w^2(n)$. Finally, in an effort to reduce the variance of the periodogram estimation, the Welch method separates the data series into N overlapping segments. As with the modified periodogram the Welch method applies a weighting window to reduce spectral leakage, but weighting is applied to each segment. Finally an averaged PSD is calculated using all segments. Power spectral density by the Welch periodogram is given by

$$P_W(f) = \frac{1}{N}\sum_{i=0}^{N-1} P_{M,i}(f) \qquad (2.13)$$

where $P_{M,i}(f)$ is the ith modified periodogram from the data series.

5.6.2 Burg Periodogram

Autoregressive spectral estimation methods differ from non-parametric methods in that they attempt to model the data instead of estimating the PSD directly. Several modeling methods exist for AR spectrum estimation, but the Burg method is the most common in HRV [2, 31, 32].

The power spectrum of a p[th] order autoregressive process is given by

$$P_{Burg}(f)=\frac{1}{f_s}\frac{\varepsilon_p}{\left|1+\sum_{k=1}^{p}a_p(k)e^{-2\pi jkf/f_s}\right|^2} \qquad (2.14)$$

where ε_p is the total least square error, f_s is the sample rate, and a_p are the Burg AR model parameters [33]. Boardman, et al. suggests that a model order of p=16-20 is a sound choice for HRV in human IBI resampled at 2-4 Hz [34].

5.6.3 Lomb-Scargle Periodogram

As mentioned before the Lomb-Scargle periodogram (LSP) method of estimating PSD does not require resampling. The LSP only uses available data. Conceptually LSP estimates the frequency spectrum by performing a least squares fit of sinusoids to the data. Unlike Welch's periodogram weighted windowing functions are not applied to data in LSP because standard weighting methods cannot be applied to unevenly sampled data. The LSP of a non-uniformly sampled, real-valued data sequence *X* of length *N* for arbitrary times t_n is defined by

$$P_{LS}(f)\equiv\frac{1}{2\sigma^2}\left\{\begin{array}{l}\dfrac{\left[\sum_{n=1}^{N}\left(X(t_n)-\overline{X}\right)\cos\left(2\pi f(t_n-\tau)\right)\right]^2}{\sum_{n=1}^{N}\cos^2\left(2\pi f(t_n-\tau)\right)}\\ +\dfrac{\left[\sum_{n=1}^{N}\left(X(t_n)-\overline{X}\right)\sin\left(2\pi f(t_n-\tau)\right)\right]^2}{\sum_{n=1}^{N}\sin^2\left(2\pi f(t_n-\tau)\right)}\end{array}\right\} \qquad (2.15)$$

where $\bar{x}$ and σ^2 are the mean and variance of the time series, and $\tau\equiv\tan^{-1}\left(\left(\sum_{n=1}^{N}\sin(4\pi ft_n)\right)/\left(\sum_{n=1}^{N}\cos(4\pi ft_n)\right)\right)$. τ is a frequency dependent time delay, defined to make the periodogram insensitive to time shift[24-26]. A more detailed description of the LSP appears in [25, 35]. Clifford, et al. showed that ectopic beat removal of up to 20% of the data points in an IBI signal does not introduce a "significant" error in frequency-domain HRV measures based on LSP [23]. Because of the resistance to errors from data removal and resampling, LSP could be the preferred power spectrum

estimation method for HRV. Comparison of the Welch, Burg, and Lomb-Scargle (LS) periodograms are presented in Figure 5.4.

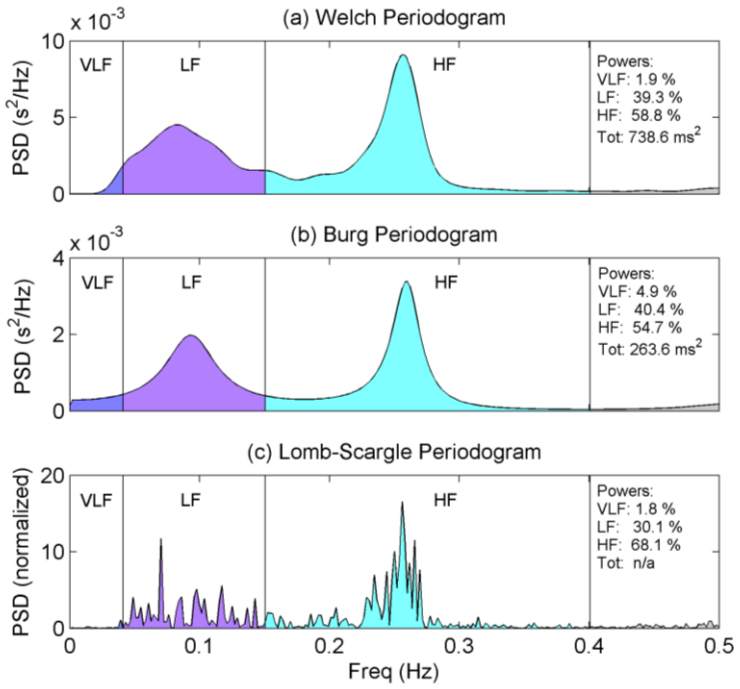

Figure 5.4 – Comparison of PSD estimates. Estimates include (a) Welch periodogram, (b) Burg autoregressive periodogram, and (c) Lomb-Scargle periodogram estimates. HRV frequency bands are labeled as very low frequency (VLF, 0-0.04 Hz), low frequency (LF, 0.04-0.15 Hz), and high frequency (HF, 0.15-0.4 Hz). PSD's computed using preprocessed IBI from healthy human. Powers represent percent of total power.

5.7 Time-Frequency Analysis

HRV analysis by means of frequency-domain methods can only yield information about how IBI signal power is distributed in the frequency domain. They provide no insight into the temporal evolution of the spectrum. Methods used to allow simultaneous viewing of both time and frequency information are often termed time-frequency analysis. Like frequency-domain analysis, time-frequency HRV analysis quantifies VLF,

LF, and HF related measures. The two primary types of time-frequency analysis used are the windowed Fourier transform (also called short-time Fourier transform, STFT) and the continuous wavelet transform [36]. To include spectral estimation methods other than the Fourier transform, the term windowed periodogram will be used in place of windowed Fourier transform. This generalization allows the inclusion of the windowed Burg periodogram and windowed Lomb-Scargle periodogram.

5.7.1 Windowed Periodogram

The windowed power spectrum is an extension of the basic PSD. As the term implies, the data is broken down into consecutive (overlapping or not) segments or windows. The PSD is then computed for each segment. This is similar to the technique use by Bartlett and Welch. However, those methods lose any temporal information by averaging all PSD's into a single PSD. Unlike Welch's method, the windowed periodogram can use other techniques to compute the PSD, e.g. Burg periodogram. Plotting PSD values onto a two-dimensional plane with frequency and time as the vertical and horizontal axes respectively produces a spectrogram (Figure 5.5).

Two alternatives are the windowed Burg periodogram and the windowed Lomb-Scargle periodogram [37, 38]. For the windowed Burg periodogram the entire data series is first resampled and then broken into segments of equal lengths. Finally, the PSD is computed for each segment using the Burg periodogram.

The windowed Lomb-Scargle periodogram is computed in almost the same manner. First, the data is broken into segments of equal lengths of time [26]. Due to the uneven sampling of IBI's, each segment can contain differing number of data points. Finally, the LSP for each segment is computed.

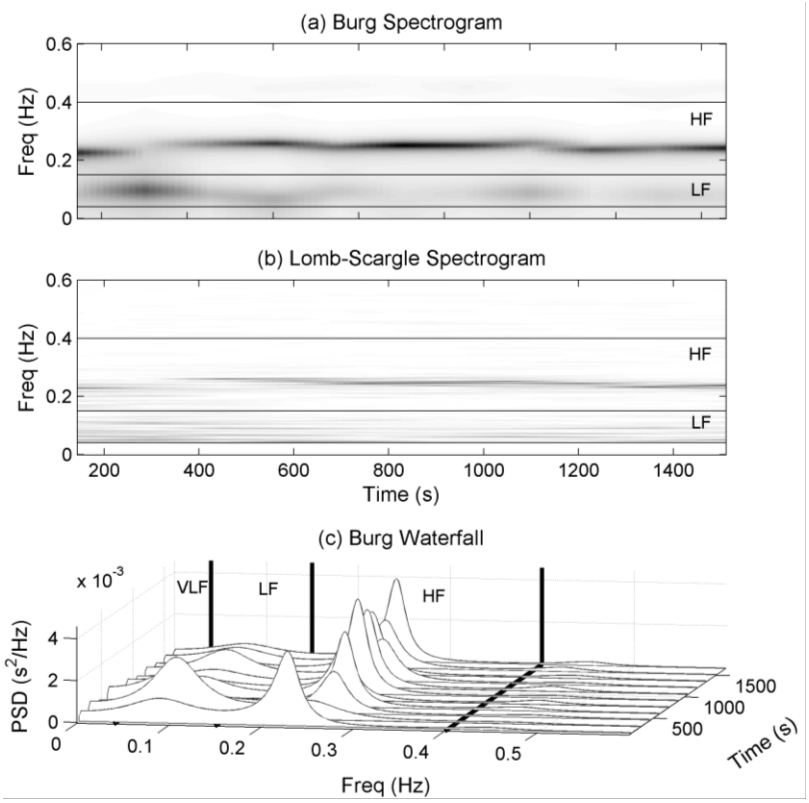

Figure 5.5 – Spectrogram and waterfall plot for windowed periodograms. Plots generated using preprocessed IBI from healthy human. Plots include (a) Spectrogram using windowed Bug periodogram. (b) Spectrogram using windowed LSP (c) Waterfall plot containing Burg periodograms of each five minute segment of IBI.

HRV quantification from time-frequency analysis using windowed periodograms can be accomplished two ways. The first method computes an averaged or global power spectrum and then calculates typical frequency-domain HRV measures ,e.g., LF, HF, LFHF. Averaging the power spectrum eliminates any time resolution and defeats some of the purpose of time-frequency analysis, but it provides a way to help control variances by averaging many power spectrums [39]. Alternatively, HRV measures can be calculated for each segment, and then an average HRV measure computed. The second method produces discretely instantaneous frequency-domain measures that are a function of time, e.g., LF(t) and LFHF(t).

From the LFHF instantaneous time series, another index can be extracted called the ratio of LFHF ratios (rLFHF) [37]. This measure represents the "global" sympathetic-parasympathetic equilibrium [37]. Imagine a line drawn through LFHF =1 on the instantaneous LFHF plot. Above this line (LFHF >1) there is a sympathetic dominance. Below this line (LFHF <1) there is a parasympathetic dominance. The rLFHF ratio is obtained by calculating the ratio of the bounded area above the line LFHF=1 to the bounded area below.

5.7.2 Wavelet Transforms

Wavelet transforms are a relatively recent, but enormously popular tool for analyzing and compressing many types of time signals. The term wavelet implies a small wave and is of finite length and energy [40]. Like Fourier transform the wavelet transform separates a signal into its fundamental components. However, unlike the Fourier transform, wavelet transforms can be applied to non-stationary signals and are not limited to a single set of basis waveforms for signal decomposition. Fourier transforms rely on the sinusoid waveform, whereas wavelet transforms have an infinite set of basis waveforms or mother wavelets as long as they satisfy predefined mathematical criteria. This property may provide access to information that could be obscured by methods like Fourier analysis [41]. Acharya, et al. state that "bio-signals usually exhibit self-similarity patterns in their distribution, and a wavelet which is akin to its fractal shape would yield the best results in terms of clarity and distinction of patterns. [41]"

The following summary of Acharya's [2] understanding of wavelet transform concepts provides an efficient explanation. The wavelet transform correlates a mother wavelet with sections of the original signal to produce wavelet coefficients. The mother wavelet is shifted/translated in time to generate a set of coefficients along the time signal. Next the mother wavelet is contracted or dilated to create coefficients along the time series at varying time scales. Here the term scale is analogous to frequency or more precisely the pseudo frequency (average frequency). Scaled wavelets are normalized so each one contains the same amount of energy. The scale can be thought of as the wavelet width and the translation as its location in time. Larger scale values represent smaller wavelet size and thus higher frequencies.

This research is concerned with the continuous wavelet transform (CWT), the discrete wavelet transform (DWT), and discrete wavelet packet transform (DWPT). The major differences between the three are how the wavelet function is scaled and translated.

5.7.2.1 Continuous Wavelet Transform

For a given signal *x(t)* and wavelet function $\psi_{a,b}(t)$, the CWT coefficients are given by

$$W(\tau,\alpha)=\frac{1}{\sqrt{\alpha}}\int_{-\infty}^{\infty}x(t)\psi^{*}\left(\frac{t-\tau}{\alpha}\right)dt \qquad (2.16)$$

where $\psi^{*}(t)$ is the complex conjugate of the mother wavelet $\psi(t)$, α is the dilation parameter, and τ is the location parameter. The bivariant function W(τ,α) shows the similarity of *x(t)* to a wavelet scaled by α at a given time τ *[20]*. Theoretically the CWT wavelet coefficients are calculated for infinitesimally small translations and scale factors. However, practical implementations of the CWT must balance the number of translations and scales to produce acceptable computational times. Most programmatic implementations of the CWT allow the user to specify the number of scales to use for computation. Plotting CWT coefficients onto a two-dimensional plane with scale and location as the vertical and horizontal axes produces a scalogram.

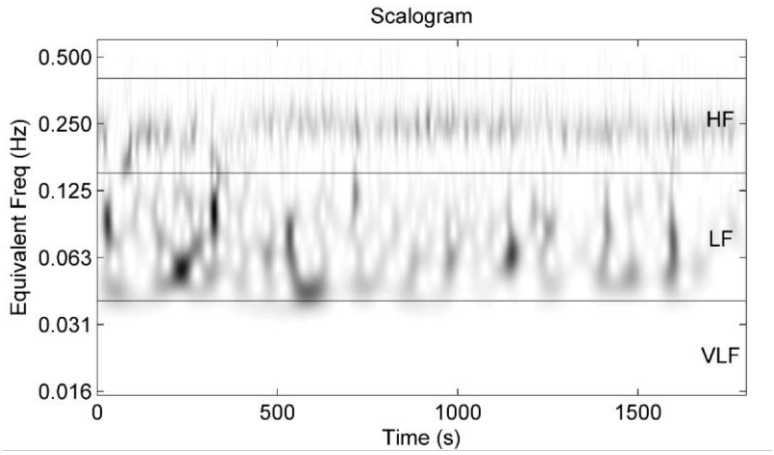

Figure 5.6 – CWT scalogram of IBI data. CWT computed using preprocessed IBI from healthy human with DOG2 wavelet [42]. The frequency axis is displayed using a log scale and represents the equivalent frequency of CWT scales [42].

5.7.2.2 Discrete Wavelet Transform

In the case of DWT and DWPT, the scaling and translations are done in a less smooth or more discrete manner. Scaling and translating for the DWT are based on powers of 2 or dyadic blocks, e.g., 2^1, 2^2, etc. The dilation function is often represented as a tree of low and high pass filters. The first step of the tree decomposes the original signal into detail (high frequency) and approximation (low frequency) components. Detail and approximation components for three levels of decomposition are represented in Figure 5.7-a by A and D. Only the approximations are further split into finer components in the DWT. For DWPT both branches of the tree are split into finer components. Figure 5.7-b shows the tree for DWPT for 3 levels of decomposition.

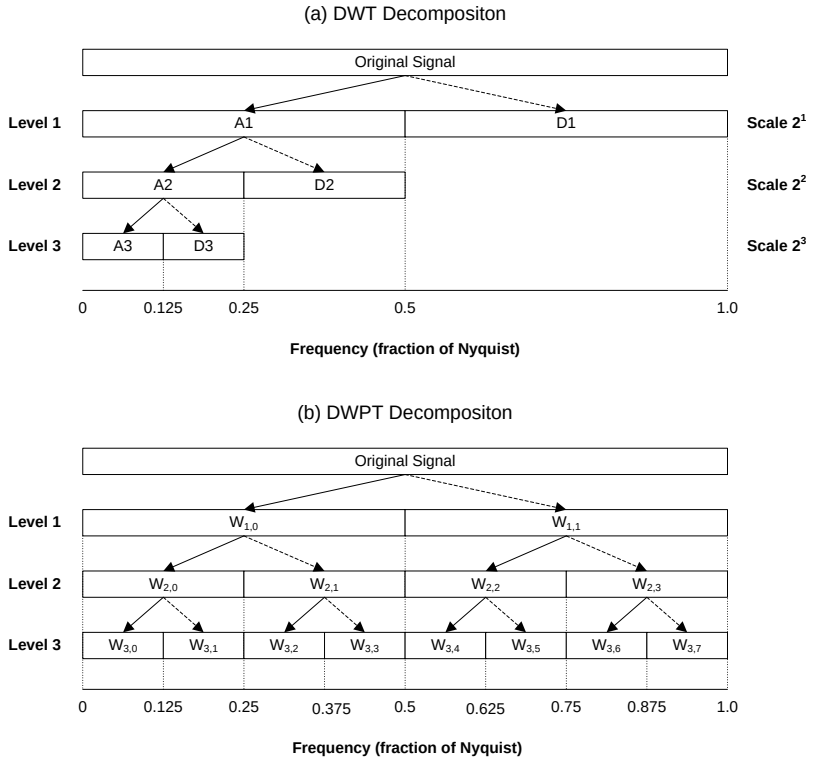

Figure 5.7 – DWT decomposition tree. Decomposition trees showing the breakdown of an arbitrary original signal into three levels using (a) discrete wavelet transform and (b) wavelet packet transform. Horizontal axis shows frequency range as a fraction of the Nyquist frequency. DWPT can extract all frequency bands with equal resolution. Diagram modified from Tanaka and Hargens [43].

Quantification of HRV measures from time-frequency analysis by CWT is accomplished in a similar manner to that employed for the windowed periodogram. Similar in that both can use either the instantaneous or global power spectrums [44]. To obtain HRV measures using instantaneous power methods, the squared modulus of the wavelet coefficients is integrated over the desired frequency band $[f_1\ f_2]$. To integrate over a frequency band wavelet scales must be changed to frequencies. The time-scale map (scalogram) must be interpreted in terms of a time-frequency map (spectrogram). The instantaneous power of the frequency band $[f_1\ f_2]$ is given by

$$P_{CWT}(t) = \frac{1}{C_\Psi}\int_{\alpha_1}^{\alpha_2} |W(t,\alpha)|^2 \frac{d\alpha}{\alpha^2} = \frac{1}{C_\Psi f_\Psi}\int_{f_1}^{f_2} |W(t, f_\Psi / f)|^2 df. \qquad (2.17)$$

The wavelet equivalent to an averaged periodogram is the global wavelet spectrum and is given by

$$\overline{W}^2(t) = \frac{1}{N}\sum_{n=0}^{N-1} |W_n(t)|^2 \qquad (2.18)$$

5.7.3 Nonlinear Analysis

On the basis that HR control may contain nonlinear components, there is an increasing interest to study HRV using methods other than the standard linear methods, i.e., time-domain and spectral analysis. These methods are often included under the umbrella term nonlinear HRV analysis. It has been shown that loss of IBI signal complexity [5, 45] and loss of fractal like scaling behaviors [46, 47] may be a general feature of cardiac pathology. Poincaré plot analysis, entropy based measures, and fractal based measures are but a few HRV analysis techniques used.

5.7.4 Poincaré Plot

The Poincaré plot or first-return map, named after Henry Poincaré, is a plot of IBI intervals versus the previous IBI interval. Poincare plots are a type of nonlinear analysis used to quantify self-similarity [48]. HRV measures based on Poincaré plots are based on the idea that each IBI is influenced by the previous one [49]. Thus, pairs of successive IBI form an attractor in the Poincare' plot. Often an ellipse is fitted to the plotted data with the long axis along the line of identity defined by $y = x$. Figure 5.8 illustrates the Poincare' plot generated using healthy human IBI data. If the center or attractor of the ellipse is located at the mean IBI ($\overline{IBI}$), then $y = -x + 2\overline{IBI}$ defines the line perpendicular to the line of identify and passing through the mean [50]. Points above the line of identity indicate a longer IBI than the preceding IBI, and points below the line of identity indicate a shorter IBI than the preceding. Standard deviations along the line of identity (SD2) and perpendicular to the line of identity (SD1) represent the magnitude of the major and minor axes of the ellipse respectively. SD1 represents the SD of the instantaneous beat-to-beat variability or short term variability. SD2 represents the SD of the continuous or long-term variability [48, 51]. In reality the ellipse is primarily a visual aid and the numerical values of the standard deviations SD1 and SD2 contain the important data. Also, the ratio of SD1 to SD2 has been suggested to be strongly associated with mortality in adults with postoperative ischemia [52, 53].

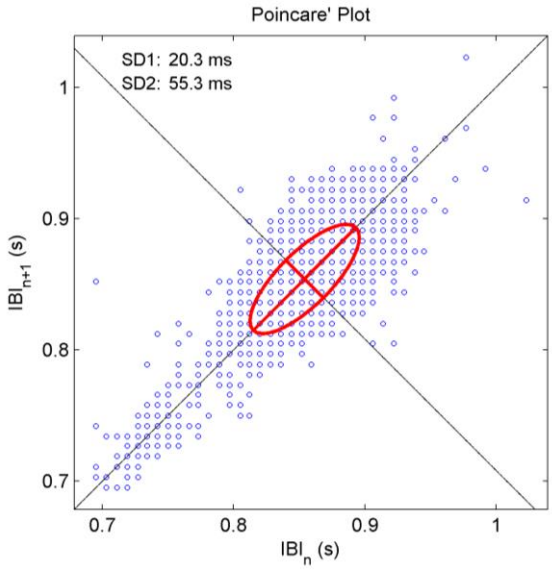

Figure 5.8 – Poincare' Plot using healthy human IBI data.

5.7.5 Sample Entropy

Sample entropy (sampen) is an embedded entropy that attempts to quantify a signal's complexity or rate of new information generation [54]. To understand how sample entropy is calculated a few definitions follow. Let $X_i=\{x_1,\ldots, x_i,\ldots x_N\}$ represent the original *N*-long IBI series. Let $\mathbf{u}_{m+1}[i]=\{x_i,x_{i+1},\ldots,x_{i+m}\}$ and $\mathbf{u}_m[i]=\{x_i,x_{i+1},\ldots,x_{i+m-1}\}$ represent *m+1* and *m* length vectors/sequences taken from *X*. Also, let the distance *d* be the maximum absolute distance between the components of two vectors and is given by

$$d(\mathbf{u}[i],\mathbf{u}[j])=\max\left(\left|\mathbf{u}[i+k]-\mathbf{u}[j+k]\right|:0\le k\le m-1\right).$$

For each i ≤ N-m a template vector $\mathbf{u}_m[i]$ is compared to all other m length vectors $\mathbf{u}_m[j]$ where i ≠ j and j ≤ N-m. The number of j that satisfy d(u[i],u[j]) ≤ r is set as n_i^m. The unconditional probability of randomly selecting two *m* length sequences from a signal that have a distance less than *r* using the relative frequency methods is $C_i^m=n_i^m/(N-m)$. Furthermore the averaged probability is given by

$$\phi^m(\mathrm{r}) = (\mathrm{N\text{-}m})^{-1} \sum_{i=1}^{N-m} C_i^m \qquad (2.19)$$

Similarly n_i^{m+1}, C_i^{m+1}, and ϕ^{m+1} are calculated for vector lengths of m+1. Finally sample entropy is determined by

$$SampEn(m, r, N) = -\ln\left[\phi^{m+1}(r) / \phi^m(r)\right] \qquad (2.20)$$

Fundamentally, sample entropy can be described as the negative logarithm of the conditional probability of randomly selecting two *m*-length sequences, from a signal, that have a distance less than *r* between them given that they also have a distance less than *r* if their lengths are increased to *m+1*. If the sample entropy is zero, then consecutive sequences are identical. Larger values of sample entropy represent higher complexity.

5.7.6 Detrended Fluctuation Analysis

Fractal scaling or self-similarity are concepts based on the idea that a system or shape can be fragmented into smaller parts where each part resembles one another but on different scales [1]. The Sierpenski triangle is classic example of fractal geiometry. A few examples of fractals occurring in nature include snowflakes, shorelines, crystals, and some ferns. For the case of IBI, the scale is time. Detrended fluctuation analysis (DFA) [55] tries to quantify the fractal like or self-similar properties of non-stationary time series [56, 57]. “This technique is a modification of root-mean-square analysis of random walks applied to non-stationary signals” [58]. The root-mean-square fluctuation of an integrated and detrended time series is measured at different scales and plotted against the size of the scale onto a log-log plot (see Figure 5.9).

First consider an IBI time series of length *N*. The IBI series is integrated using

$$y(k) = \sum_{i=1}^{k}\left[IBI(i) - \overline{IBI}\right] \qquad (2.21)$$

where y(k) is the kth value of the integrated series, IBI(i) is the i^{th} interbeat interval, and $\overline{IBI}$ is the average interbeat interval for the entire time series. The integrated time series is then separated into segments of length n. A least squares line is fit to the data in each segment to define the local trend denoted by $y_n(k)$. Next, the integrated time series is detrended by subtracting the local trend, $y_n(k)$ from each segment. Finally, the root-mean-squared fluctuation of the integrated and detrended time series is calculated by

$$F(n)=\sqrt{\frac{1}{N}\left(\sum_{k=1}^{N}\left[y(k)-y_n(k)\right]^2\right)} \qquad (2.22)$$

where m represents the window or scale size. F(*m*) is computed on a user defined range of time scales. The linear relationship between log(*F*) and log(n) represents the scaling exponent, α, of the interbeat interval time series. Often two distinct linear regions on the log-log plot are used to describe the short term scaling, α_1, and the long term scaling, α_2[57]. These two regions are separated by a breakpoint located around 12-16 beats [57]. Figure 5.9 shows the DFA plot for a typical human IBI signal with a break point at 12 beats.

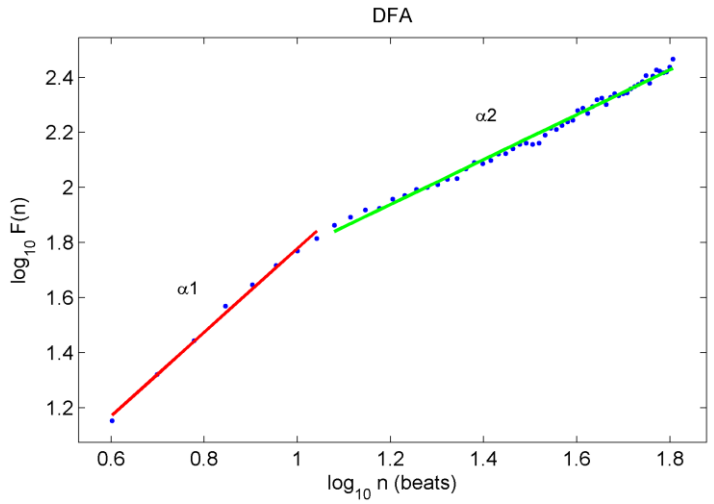

Figure 5.9 – Detrended fluctuation analysis using healthy human data. Short term scaling exponent and long term scaling exponents are represented by α1 and α2. The breakpoint is located at 12 beats.

1. Seely, A.J. and P.T. Macklem, *Complex systems and the technology of variability analysis.* Crit Care, 2004. **8**(6): p. R367-R384.
2. Acharya, U.R., et al., *Heart rate variability: a review.* Med Biol Eng Comput, 2006. **44**(12): p. 1031-1051.
3. Berntson, G.G., et al., *Heart rate variability: Origins, methods, and interpretive caveats.* Psychophysiology, 1997. **34**(6): p. 623-648.
4. Malik, M., et al., *Heart Rate Variability : Standards of Measurement, Physiological Interpretation, and Clinical Use.* Circulation, 1996. **93**(5): p. 1043-1065.

5. Thuraisingham, R.A., *Preprocessing RR interval time series for heart rate variability analysis and estimates of standard deviation of RR intervals.* Comput.Methods Programs Biomed., 2006.
6. Colak, O.H., *Preprocessing effects in time-frequency distributions and spectral analysis of heart rate variability.* Digital Signal Processing, 2009. **19**(4): p. 731-739.
7. Yates, R.D., Goodman, David J., *Probabilitty and Stochastic Processes: A Friendly Introducxtion for Electrical and Computer Engineers*. Second ed. 2005, Hoboken, NJ: John Wiley & Sons, Inc.
8. Yoo, C.S., Yi, S. H. , *Effects of Detrending for Analysis of Heart Rate Variability and Applications to the Estimation of Depth of Anesthesia.* Journal of the Korean Physical Society, 2004. **44**(3): p. 561-568.
9. Tarvainen, M., *Estimation Methods for Nonstationary Biosignals*, in *Department of Applied Physics*. 2004, University of Kuopio: Kuopio, Finland.
10. Aubert, A.E., et al., *The analysis of heart rate variability in unrestrained rats. Validation of method and results.* Comput Methods Programs Biomed, 1999. **60**(3): p. 197-213.
11. Lippman, N., K.M. Stein, and B.B. Lerman, *Comparison of methods for removal of ectopy in measurement of heart rate variability.* Am J Physiol, 1994. **267**(1 Pt 2): p. H411-8.
12. Huikuri, H.V., et al., *Abnormalities in Beat-to-Beat Dynamics of Heart Rate Before the Spontaneous Onset of Life-Threatening Ventricular Tachyarrhythmias in Patients With Prior Myocardial Infarction.* Circulation, 1996. **93**(10): p. 1836-1844.
13. Huikuri, H., et al., *Frequency domain measures of heart rate variability before the onset of nonsustained and sustained ventricular tachycardia in patients with coronary artery disease.* Circulation, 1993. **87**(4): p. 1220-1228.
14. Mitov, I.P., *A method for assessment and processing of biomedical signals containing trend and periodic components.* Med Eng Phys, 1998. **20**(9): p. 660-8.
15. Shafqat, K., S.K. Pal, and P.A. Kyriacou, *Evaluation of two detrending techniques for application in Heart Rate Variability.* Conf Proc IEEE Eng Med Biol Soc, 2007. **2007**: p. 267-70.
16. Tarvainen, M.P., P.O. Ranta-Aho, and P.A. Karjalainen, *An advanced detrending method with application to HRV analysis.* IEEE Trans Biomed Eng, 2002. **49**(2): p. 172-5.
17. Juha-Pekka, N., et al., *Software for advanced HRV analysis.* Computer methods and programs in biomedicine, 2004. **76**(1): p. 73-81.
18. Singh, D., K. Vinod, and S.C. Saxena, *Sampling frequency of the RR interval time series for spectral analysis of heart rate variability.* J Med Eng Technol, 2004. **28**(6): p. 263-72.
19. Mietus, J.E., et al., *The pNNx files: re-examining a widely used heart rate variability measure.* Heart, 2002. **88**(4): p. 378-380.
20. Clifford, G.D., F. Azuaje, and P.E. McSharry, *Advanced Methods and Tools for ECG Data Analysis*. 2006, Norwood, MA: Artech House, Inc. 371.
21. JG Proakis, D.M., *Digital Signal Processing: Principles, Algorithms, and Applications*. Third ed. 1996, New Jersey: Prentice-Hall, Inc.
22. Name, N., *Needed Equation*. 0000.
23. Clifford, G.D. and L. Tarassenko, *Quantifying errors in spectral estimates of HRV due to beat replacement and resampling.* IEEE Trans Biomed Eng, 2005. **52**(4): p. 630-8.
24. C. Lévy-Leduc, E.M., F. Roueff,, *Frequency estimation based on the cumulated Lomb Scargle periodogram.* Journal of Time Series Analysis, 2008. **29**(6): p. 1104-1131.
25. Laguna, P., G.B. Moody, and R.G. Mark, *Power spectral density of unevenly sampled data by least-square analysis: performance and application to heart rate signals.* Biomedical Engineering, IEEE Transactions on, 1998. **45**(6): p. 698-715.
26. Thong, T., J. McNames, and M. Aboy, *Lomb-Wech periodogram for non-uniform sampling.* Conf Proc IEEE Eng Med Biol Soc, 2004. **1**: p. 271-4.
27. Thong T, Y.I., P Zajdel DP, Ellingson RM, McNames J, Aboy M, Oken BS. *Heart rate variability analysis of effect of nicotine using periodograms*. in *IEEE Engineering in Medicine and Biology Society*. 2004.

28. Belova, N.Y., S.V. Mihaylov, and B.G. Piryova, *Wavelet transform: A better approach for the evaluation of instantaneous changes in heart rate variability.* Auton Neurosci, 2007. **131**(1-2): p. 107-22.
29. Zhong, Y., et al., *Autonomic nervous nonlinear interactions lead to frequency modulation between low- and high-frequency bands of the heart rate variability spectrum.* Am J Physiol Regul Integr Comp Physiol, 2007. **293**(5): p. R1961-1968.
30. Pereira de Souza Neto, E., et al., *Assessment of autonomic cardiovascular indices in non-stationary data in rats.* Comparative Biochemistry and Physiology - Part A: Molecular & Integrative Physiology, 2001. **128**(1): p. 105-115.
31. Thayer, J.F., et al., *Estimating respiratory frequency from autoregressive spectral analysis of heart period.* IEEE Eng Med Biol Mag, 2002. **21**(4): p. 41-5.
32. Wijnen, V.J., et al., *Autonomic reactivity to sensory stimulation is related to consciousness level after severe traumatic brain injury.* Clin Neurophysiol, 2006. **117**(8): p. 1794-807.
33. Subasi, A., et al., *Comparison of subspace-based methods with AR parametric methods in epileptic seizure detection.* Computers in Biology and Medicine, 2006. **36**(2): p. 195-208.
34. Boardman, A. and et al., *A study on the optimum order of autoregressive models for heart rate variability.* Physiological Measurement, 2002. **23**(2): p. 325.
35. Lomb, N.R., *Least-squares frequency analysis of unequally spaced data.* Astrophysics and Space Science, 1976. **39**(2): p. 447-462.
36. Issartel, J., et al., *A practical guide to time-frequency analysis in the study of human motor behavior: the contribution of wavelet transform.* J Mot Behav, 2006. **38**(2): p. 139-59.
37. Carvalho, J.L.A., et al., *A Tool for Time-Frequency Analysis of Heart Rate Variability.*
38. Thong T, M.J., Aboy M, Oken BS. *Averaged Lomb periodograms for nonuniform sampling*. in *7th Biennial International EURASIP Conference Biosignal 2004*. 2004. Brno, Czech Republic.
39. Zhiguo, Z. and C. Shing-Chow. *Robust adaptive Lomb periodogram for time-frequency analysis of signals with sinusoidal and transient components*. in *Acoustics, Speech, and Signal Processing, 2005. Proceedings. (ICASSP '05). IEEE International Conference on*. 2005.
40. M Vetterli, C.H., *Wavelets and Filter Banks: Theory and Design.* IEEE Transactions on Signal Processing, 1992. **40**(9): p. 2207-2232.
41. Acharya, U.R., Suri, J.S., Spaan, J.A.E., Krishnan, S.M, *Advanced in Cardiac Signal Processing*. 2007, Berlin: Springer-Verlag. 468.
42. Torrence, C. and G.P. Compo, *A Practical Guide to Wavelet Analysis.* Bulletin of the American Meteorological Society, 1998. **79**(1): p. 61-78
43. Tanaka, K. and A.R. Hargens, *Wavelet packet transform for R-R interval variability.* Medical Engineering & Physics, 2004. **26**(4): p. 313-319.
44. Mainardi, L.T., *On the quantification of heart rate variability spectral parameters using time–frequency and time-varying methods.* Philosophical Transactions of the Royal Society A: Mathematical, Physical and Engineering Sciences, 2009. **367**(1887): p. 255-275.
45. Papaioannou, V.E., et al., *Investigation of altered heart rate variability, nonlinear properties of heart rate signals, and organ dysfunction longitudinally over time in intensive care unit patients.* J.Crit Care, 2006. **21**(1): p. 95-103.
46. Bojorges-Valdez, E.R. and et al., *Scaling patterns of heart rate variability data.* Physiological Measurement, 2007. **28**(6): p. 721.
47. Beckers, F., B. Verheyden, and A.E. Aubert, *Aging and nonlinear heart rate control in a healthy population*. 2006. p. H2560-2570.
48. Kamen, P.W. and A.M. Tonkin, *Application of the Poincar plot to heart rate variability: a new measure of functional status in heart failure.* Internal Medicine Journal, 1995. **25**(1): p. 18-26.
49. Lerma, C., et al., *Poincare plot indexes of heart rate variability capture dynamic adaptations after haemodialysis in chronic renal failure patients.* Clin Physiol Funct Imaging, 2003. **23**(2): p. 72-80.

50. Tulppo, M.P., et al., *Quantitative beat-to-beat analysis of heart rate dynamics during exercise.* Am J Physiol Heart Circ Physiol, 1996. **271**(1): p. H244-252.
51. Brennan, M., M. Palaniswami, and P. Kamen, *Poincare plot interpretation using a physiological model of HRV based on a network of oscillators.* Am J Physiol Heart Circ Physiol, 2002. **283**(5): p. H1873-1886.
52. Laitio, T.T., et al., *Correlation properties and complexity of perioperative RR-interval dynamics in coronary artery bypass surgery patients.* Anesthesiology, 2000. **93**(1): p. 69-80.
53. Stein, P.K. and A. Reddy, *Non-linear heart rate variability and risk stratification in cardiovascular disease.* Indian Pacing Electrophysiol J, 2005. **5**(3): p. 210-20.
54. Richman, J. and J. Moorman, *Physiological time-series analysis using approximate entropy and sample entropy.* Am J Physiol Heart Circ Physiol, 2000. **278**(6): p. H2039-2049.
55. Peng, C.K., et al., *Mosaic organization of DNA nucleotides.* Physical Review E, 1994. **49**(Copyright (C) 2010 The American Physical Society): p. 1685.
56. Voss, A., et al., *Methods derived from nonlinear dynamics for analysing heart rate variability.* Philosophical Transactions of the Royal Society A: Mathematical, Physical and Engineering Sciences, 2009. **367**(1887): p. 277-296.
57. Peng, C.K., et al., *Quantification of scaling exponents and crossover phenomena in nonstationary heartbeat time series.* Chaos, 1995. **5**(1): p. 82-7.
58. Acharya, U., Suri, JS, Spaan, JAE, Krishnan, SM, *Advances in Cardiac Signal Processing*. 2007, Berlin Heidelberg, Germany: Springer.